Eurasian J. Sci. Eng., 2025, 11(2), 235-251
https://doi.org/10.23918/eajse.v11i2p15

Published by Tishk International University
Available at: https://eajse.tiu.edu.iq/

RESEARCH ARTICLE Open Access

Numerical Study of Nonlinear Reaction-Diffusion Equation in Catalytic Pellet Model Using Finite Element Method

Hero M. Hussein[1], and Younis A. Sabawi[1*]

[1]Department of Mathematics, Faculty of Science and Health, Koya University, Koya 44023, Kurdistan Region-F. R. Iraq

Article History
Received: 03.03.2025
Revised: 01.05.2025
Accepted: 30.08.2025
Published: 01.09.2025
Communicated by: Prof. Dr. Cenap Ozel
*Email address:
younis.abid@koyauniversity.org
*Corresponding Author

Abstract: This study explores numerical solutions to nonlinear reaction-diffusion equations, with a focus on modeling concentration profiles in catalytic pellets, crucial for many chemical engineering applications. The problem is discretised and investigated in both the temporal and spatial domains using finite element method. A weak formulation is developed, and the existence and uniqueness of the finite element method solution are established. Stability and convergence of the numerical schemes are rigorously analyzed, and Crank–Nicolson-based discretization is implemented for enhanced accuracy. Numerical results illustrate the effectiveness of finite element method and finite difference method, with close agreement between the methods. This comparison highlights finite element method's potential advantages in catalytic process modeling, showcasing its effectiveness in solving nonlinear reaction-diffusion PDEs.

Keywords: *Catalytic Pellet Modeling; Numerical Analysis; Finite Element Method; Stability and Convergence.*

1. Introduction

Nonlinear partial differential equations (PDEs), are crucial in many scientific and engineering domains. Many non-linear models are challenging to solve either analytically or numerically that represent real-world problems. Solving such models often involves the inclusion of simplifying assumptions, some of which may lack full justification. One of the most adaptable and widely used methods to solve PDEs for a variety of applications in several domains is the finite element method (FEM). We will use the FEM for a numerical study in which the concentration of a reactant in a catalytic pellet was characterized by a nonlinear reaction-diffusion partial differential equation. We can write the model as follows:

$$\varepsilon \frac{\partial^2 v}{\partial x^2} - \frac{\partial v}{\partial t} = \beta v^2, \quad 0 \le x \le 1 \text{ and } 0 \le t \le T, \tag{1}$$

with initial and boundary conditions:

$$\begin{aligned} v(x,0) &= (1-x)^2, \quad 0 \le x \le 1, \\ v(0,t) &= 0, \quad 0 \le t \le T, \\ v(1,t) &= 0, \quad 0 \le t \le T. \end{aligned} \tag{2}$$

Here, $\beta > 0$ represents the reaction rate and $\varepsilon > 0$ is near zero that represents the diffusion rate. Moreover, the exact solution of the Eq. (1) is unknown, see the reference [22].

Young-Sang Cho in [19] modeled cone-shaped catalytic pellets for irreversible first-order reactions using the FEM. He found that increasing the cone angle improved effectiveness factors and analyzed hollow cone-shaped pellets in Continuous Stirblack-Tank Reactors (CSTRs). From [20] Cho, presented analytical solutions for reactant concentration in batch reactors and CSTRs with catalytic pellets of various shapes. Using reaction-diffusion equations and Laplace transforms, he examined how factors such as the shape of the pellet, diffusion, and catalyst loading affected concentration profiles.
FEM is appropriate for complicated geometries and a range of boundary restrictions since it is especially useful for managing boundary conditions and weak solutions. The formulation of the weak solution and the discretization stages in space and time using FEM, including stability analysis, are described in this study. Finite difference method (FDM) is presented as a substitute technique for verification, enabling solution comparison and FEM result validation. In [23], they presented a 3D collocation FEM for modeling flexoelectricity, implemented in Fortran with a 27-noded element. It was validated and shown to efficiently simulate complex electromechanical structures. From [26], they investigated a mixed-dimensional elliptic PDE with embedded interfaces, established well-posedness and solution regularity, developed a fitted FEM with proven error bounds, proposed a subspace decomposition iterative solver, and validated its rapid convergence through numerical experiments.
Recent advancements in numerical methods for solving PDEs have emphasized the importance of accurate error estimation and efficient computational techniques. From [2], they solved the Whitham–Broer–Kaup shallow water model using a cubic B-spline FEM. They proved solution uniqueness, derived convergence estimates, and validated the method with numerical tests, showing high accuracy in L^2 and L^∞ norms. Sabawi's contributions to a posteriori error analysis provide critical insights into finite element approximations for fully discrete semilinear parabolic problems, as demonstrated in both [8] and [9]. His work establishes error bounds in $L^\infty(H^1)$ norms, enhancing the reliability of FEMs for complex problems. Additionally, the collaborative efforts of Sabawi et al. in developing high-order solutions for PDEs, such as the Generalized Burgers–Fisher equation [10] and the diffusive Lotka–Volterra system [11], illustrate the power of compact finite difference and implicit-explicit Runge-Kutta methods. Moreover, Sabawi's exploration of semilinear parabolic integro-differential equations [13, 12, 16] highlights the applicability of posteriori error bounds in diverse mathematical models, offering robust tools for tackling challenging systems in applied sciences.
The motivation for this study stems from the need to develop robust numerical techniques for solving nonlinear reaction-diffusion equations that model catalytic processes. While FDM have been applied to such problems [22], the FEM offers advantages in handling complex geometries and boundary conditions. This research aims to provide a comprehensive theoretical foundation for FEM application to catalytic pellet models, including existence and uniqueness proofs, stability analysis, and convergence estimates, while comparing its performance with established FDM approaches.

2. Semi-Discrete Galerkin Scheme

Consider an open set $\Omega \subset \mathbb{R}$ being bounded, and assume that all the functions presented in this study have real values. The space $C_c^\infty(\Omega)$ comprises infinitely differentiable functions that possess compact support inside Ω. The standard notation for Sobolev spaces is $W_p^r(\Omega)$; see [17] for further details. The Hilbert spaces are the Sobolev spaces $W_2^r(\Omega)$ for $p = 2$, which are denoted by $H^r(\Omega)$ to indicate their specific structure in this context. In $\mathbb{R}$, $D^\eta \psi$ represents the ηth derivative of ψ. For H^r, the norm and semi-norm are represented by $\|\cdot\|_r$ and $|\cdot|_r$ and provided by:

$$\|\psi\|_r = \left(\sum_{|\eta| \le r} \int_\Omega (D^\eta \psi)^2 d\Omega \right)^{1/2}, \quad |\psi|_r = \left(\sum_{|\eta| = r} \int_\Omega (D^\eta \psi)^2 d\Omega \right)^{1/2}.$$

We are especially interested in the space $H^1(\Omega)$ for $r=1$. The $H_0^1(\Omega)$ represents the completeness of $C_c^\infty(\Omega)$ in H^1 norm; in other words, $H_0^1(\Omega)$ includes those functions of $H^1(\Omega)$ that disappear at the boundary $\partial\Omega$. We shall write $\|\cdot\|$ for $\|\cdot\|_{L^2(\Omega)}$ for convenience. $(\cdot,\cdot)$ represents the inner product on L^2, whereas $\langle\cdot,\cdot\rangle$ represents the duality product on Hilbert spaces. $L^q(0,T;W_p^r(\Omega))$ is a representation of time dependent Sobolev spaces, which have the following formula:

$$L^q(0,T;W_p^r(\Omega)) = \left\{ \psi : (0,T) \to W_p^r(\Omega) \text{ s.t. } \psi \text{ is measurable and } \int_0^T \|\psi(t)\|_{W_p^r(\Omega)}^q dt < \infty \right\}$$

for any integer $r \geq 0$, $1 \leq q < \infty$, $1 \leq p \leq \infty$, using the subsequent norm,

$$\|\psi\|_{L^q(\Omega)} = \left(\int_0^T \|\psi(t)\|_{W_p^r(\Omega)}^q dt \right)^{1/q}, \text{ and } \|\psi\|_{H^1(\Omega)} = \left(\|\psi\|_{L^2(\Omega)}^2 + \|\frac{\partial \psi}{\partial t}\|_{L^2(\Omega)}^2 \right)^{1/2}.$$

This space consists of functions ψ that exhibit both spatial and temporal regularity.
It is important to emphasize that the time-dependent norms $L^2(0,T;H^r(\Omega))$ should not be conflated with the standard spatial norm $L^2(\Omega)$. While $L^2(\Omega)$ measures integrability strictly over the spatial domain Ω, the norms $L^2(0,T;H^r(\Omega))$ represent integrability in both the temporal and spatial sense, accounting for the time evolution of the function over $(0,T)$ and the H^r-based spatial regularity on Ω.
Our use of some significant inequalities, like Young's inequality, Cauchy-Schwarz inequality, Poincaré's inequality, Gronwall's inequality, generalized Hölder's inequality, etc., is based on PDEs [14] and the standard text of functional analysis [21, 18].
Multiply (1) by a weight function $w \in H_0^1(\Omega)$, and integrated over Ω w.r.t. x to give the weak formulation of the problem (1).

$$\int_0^1 (\varepsilon \frac{\partial^2 v}{\partial x^2} w - \frac{\partial v}{\partial t} w - \beta v^2 w)\, dx = 0. \tag{3}$$

Using integration by parts on the term involving $\frac{\partial^2 v}{\partial x^2}$, and $v(0,t)=0$ and $v(1,t)=0$. Therefore, the Equation (3) can be written as:

$$\int_0^1 (\varepsilon \frac{\partial v}{\partial x}\frac{\partial w}{\partial x} + \frac{\partial v}{\partial t} w + \beta v^2 w)\, dx = 0. \tag{4}$$

If we take $(\gamma f, g) = \int_0^1 \gamma f(x,t) g(x,t)\, dx$, then equation (4) will gives us the following weak formulation:

$$(\frac{\partial v}{\partial t}, w) + \varepsilon(\frac{\partial v}{\partial x}, \frac{\partial w}{\partial x}) + \beta(v^2, w) = 0, \tag{5}$$

with the initial condition

$$(v(0,x), w) = (v_0(x), w). \tag{6}$$

Let $S_h(\Omega), 0 < h < 1$, be a finite-dimensional subspace of $H_0^r(\Omega)$.
A semi-discrete finite element Galerkin formulation of (5) is then defined as: find $v_h = v_h(x,t)$ belonging to S_h, such that

$$(\frac{\partial v_h}{\partial t}, w) + \varepsilon(\frac{\partial v_h}{\partial x}, \frac{\partial w}{\partial x}) + \beta(v_h^2, w) = 0, \tag{7}$$

with the initial condition

$$v_h(0) = v_{0h}, \forall w \in S_h, \tag{8}$$

where v_{0h} is an approximation of v_0 in S_h.

2.1. Existence and Uniqueness

In this section, we will discuss the existence and uniqueness of the solution of the semi-discrete formulation (7) with (8).

Theorem 2.1.1. *There exists a unique solution of the semi-discrete formulation* (7) *with* (8) *for any* $T > 0$ *such that*

$$v \in L^{\infty}(0,T;H_0^1(\Omega)) \text{ with } (v(x,0),w) = (v_0,w),\ w \in H_0^1(\Omega),$$

if $v_0 \in H_0^1(\Omega)$ *for any* $T > 0$.

Proof. Let $\{\phi_i\}_{i=1}^{\infty}$ be an orthogonal basis for $H_0^1(\Omega)$ and let $U^m = \text{span}\{\phi_1, \phi_2, \ldots, \phi_m\}$, we define

$$v_h^m = \sum_{i=1}^{m} \alpha_i(t)\varphi_i \tag{9}$$

for each $t > 0$ that satisfies

$$(\frac{\partial v_h^m}{\partial t}, w) + \varepsilon(\frac{\partial v_h^m}{\partial x}, \frac{\partial w}{\partial x}) + \beta((v_h^m)^2, w) = 0, \tag{10}$$

with $v^m(0) = v_{0,m}$, where

$$v_{0,m} = v^m(0) = \sum_{i=1}^{m} \alpha_i(0)\phi_i = P^m v_0,$$

where P^m is an orthogonal projection on to finite dimensional space U^m, and $v_{0,m} \to v_0 \in H_0^1(\Omega)$ [4, 5]. Hence (10) can be written as a system of first order non-linear ordinary differential equation and there exists a positive time $t_m > 0$ such that the nonlinear system has a unique solution v^m over $(0,t_m)$. Hence, v_h^m can be defined by the standard existence and uniqueness theorem for system of ODEs [6]. Thus there exist $v_h^m \in S_h(\Omega)$ and $t_n \in (0,T]$.
To prove uniqueness, for easier analysis, we present the semi-discrete (7), as follows:

$$(\frac{\partial v_h}{\partial t}, w) + \varepsilon(\frac{\partial v_h}{\partial x}, \frac{\partial w}{\partial x}) + \beta(f(v_h), w) = 0, \text{ where } f(v_h) = v_h^2. \tag{11}$$

Let v_h and $\tilde{v_h}$ be two solutions of (11) and take $V = v_h - \tilde{v_h}$, and subtracting the two resulting equations leads to

$$(\frac{\partial V}{\partial t}, w) + \varepsilon(\frac{\partial V}{\partial x}, \frac{\partial w}{\partial x}) + \beta(f(v_h) - f(\tilde{v_h}), w) = 0. \tag{12}$$

Choose $w = V$ in (12), we get

$$(\frac{\partial V}{\partial t}, V) + \varepsilon(\frac{\partial V}{\partial x}, \frac{\partial V}{\partial x}) + \beta(f(v_h) - f(\tilde{v_h}), V) = 0. \tag{13}$$

Using the Cauchy–Schwarz inequality, we conclude that

$$\frac{1}{2}\frac{d}{dt}\|V\|^2 + \varepsilon\|\frac{\partial V}{\partial x}\|^2 \le \beta\|f(v_h) - f(\tilde{v_h})\|\|V\|. \tag{14}$$

So, we have

$$\frac{1}{2}\frac{d}{dt}\|V\|^2 \le \beta\|f(v_h) - f(\tilde{v_h})\|\|V\|. \tag{15}$$

We need to show that f is locally Lipschitz. From the definition of f, we have

$$|f(v_h) - f(\tilde{v_h})| = |v_h^2 - \tilde{v_h}^2| \leq (|v_h| + |\tilde{v_h}|)|v_h - \tilde{v_h}| \leq C|v_h - \tilde{v_h}|, \tag{16}$$

where C denotes a constant. Throughout this work, C will represent a generic constant and does not depend on h, which may take different values in different contexts. Now, we can show that

$$\|f(v_h) - f(\tilde{v}_h)\|^2 = \int_\Omega |v_h^2 - \tilde{v}_h^2|^2 dx \leq C \int_\Omega |v_h - \tilde{v}_h|^2 dx \leq C\|v_h - \tilde{v}_h\|^2 \leq C\|V\|^2. \tag{17}$$

Thus, (15) becomes

$$\frac{d}{dt}\|V\|^2 \leq C\|V\|^2 \tag{18}$$

Integrating form 0 to t, we can blackuce Equation (18) to

$$\|V(t)\|^2 \leq \|V(0)\|^2 + C\int_0^t \|V(s)\|^2 ds. \tag{19}$$

Applying Gronwall's inequality, we get:

$$\|V(t)\|^2 \leq \|V(0)\|^2 e^{Ct} = 0. \tag{20}$$

We see that $V(t) = 0$, this means that $v_h(t) = \tilde{v}_h(t), \forall t \in [0, T]$.

2.2. Stability and Convergence

In this section, we will discuss the conservation of energy for the solution of the semi-discrete formulation (7) with (8), which implies the stability of the numerical solution to (7). The convergence of the solution for (7) will also be consideblack.

Theorem 2.2.1. *Let $v_h \in S_h$ be the solution of* (7)*. Then there exists a constant C, independent of h such that*

$$\|v_h\|_{L^\infty(L_2(\Omega))} \leq C\|v_0\|$$

Proof. Taking $w = v_h$ in (7), we obtain

$$(\frac{\partial v_h}{\partial t}, v_h) + \varepsilon(\frac{\partial v_h}{\partial x}, \frac{\partial v_h}{\partial x}) + \beta(f(v_h), v_h) = 0, \text{ where } f(v_h) = v_h^2. \tag{21}$$

Applying Cauchy-Schwarz inequality, leads to

$$\frac{1}{2}\frac{d}{dt}\|v_h\|^2 + \varepsilon\|\frac{\partial v_h}{\partial x}\|^2 \leq \beta\|f(v_h)\|\|v_h\|. \tag{22}$$

So, we have

$$\frac{1}{2}\frac{d}{dt}\|v_h\|^2 \leq \beta\|f(v_h)\|\|v_h\|. \tag{23}$$

Now, apply the similar steps of (16), we have

$$\|f(v_h)\| = \|f(v_h) - f(0)\| \leq C\|v_h - 0\| = C\|v_h\|. \tag{24}$$

Put (24) in (23), we get

$$\frac{d}{dt}\|v_h\|^2 \leq C\|v_h\|^2. \tag{25}$$

Integrating form 0 to t, we can blackuce Equation (25) to

$$\|v_h(t)\|^2 \leq \|v_h(0)\|^2 + C\int_0^t \|v_h(s)\|^2 ds. \tag{26}$$

Using Gronwall's inequality, gives

$$\|v_h(t)\|^2 \leq C\|v_h(0)\|^2 e^{CT} \leq C\|v_h(0)\|^2. \tag{27}$$

Which implies

$$\sup_{t\in[0,T]} \|v_h(t)\| \leq C\|v_0\|. \tag{28}$$

Therefore, we have

$$\|v_h(t)\|_{L^\infty(L_2(\Omega))} \leq C\|v_0\|. \tag{29}$$

Now we analyze the accuracy of the semi-discrete scheme (7). For all $u, v \in H_0^1$ satisfies the boundedness property

$$|(\frac{\partial u}{\partial x}, \frac{\partial v}{\partial x})| \leq M\|u\|_{H^1}\|v\|_{H^1}, \forall u, v \in H_0^1 \tag{30}$$

and coercivity property (on Ω)

$$(\frac{\partial v}{\partial x}, \frac{\partial v}{\partial x}) \geq \alpha\|v\|_{H^1}, \forall v \in H_0^1, \text{ for some } \alpha \in \mathbb{R}. \tag{31}$$

Also, satisfies

$$(\frac{\partial (v-\tilde{v})}{\partial x}, \frac{\partial w}{\partial x}) = 0,\ w \in S_h, \tag{32}$$

where $\tilde{v}$ is an auxiliary projection of v [4]. Now we have the following bound for error in the semi-discrete approximation.

Theorem 2.2.2. *[3] Assuming that a function u satisfies*

$$u \in L^\infty\big(H^r(\Omega)\big),\ \frac{\partial u}{\partial t} \in L^\infty\big(H^r(\Omega)\big),$$

then there holds the following inequalities:

$$\|\tilde{u} - u\| + h\|\nabla(\tilde{u} - u)\| \leq C_1 h^r \|u\|_r, \tag{33a}$$

$$\left\|\frac{\partial(\tilde{u}-u)}{\partial t}\right\| + h\left\|\nabla\left(\frac{\partial(\tilde{u}-u)}{\partial t}\right)\right\| \leq C_2 h^r \left\|\frac{\partial u}{\partial t}\right\|_r, \tag{33b}$$

where C_1 and C_2 are constants independent of h.

Theorem 2.2.3. *If $v_h \in S_h$ is a solution of (7) and $v \in H_0^r(\Omega)$ is a solution of (5), then*

$$\|v - v_h\| \leq Ch^r, \text{ for some } C > 0.$$

Proof. Let the error be

$$e = v_h - v = (v_h - \tilde{v}) + (\tilde{v} - v) = \theta + \rho, \tag{34}$$

where $\rho = v_h - \tilde{v}$ and $\theta = \tilde{v} - v$.
Now, subtracting (5) from (7) yields

$$(\frac{\partial}{\partial t}(v_h - v), w) + \varepsilon(\frac{\partial}{\partial x}(v_h - v), \frac{\partial w}{\partial x}) + \beta(f(v_h) - f(v), w) = 0. \tag{35}$$

So, we have

$$(\frac{\partial}{\partial t}(\theta + \rho), w) + \varepsilon(\frac{\partial}{\partial x}(\theta + \rho), \frac{\partial w}{\partial x}) + \beta(f(v_h) - f(v), w) = 0. \tag{36}$$

Using (32) in (36), we get

$$(\frac{\partial \theta}{\partial t}, w) + \varepsilon(\frac{\partial \theta}{\partial x}, \frac{\partial w}{\partial x}) = (-\frac{\partial \rho}{\partial t}, w) + \beta(f(v) - f(v_h), w). \tag{37}$$

Set $w = \theta$ in (37) and using Cauchy–Schwarz inequality, we get

$$\frac{1}{2}\frac{d}{dt}\|\theta\|^2 + \varepsilon\|\frac{\partial \theta}{\partial x}\|^2 \leq \|\frac{\partial \rho}{\partial t}\|\|\theta\| + \beta\|f(v_h) - f(v)\|\|\theta\|. \tag{38}$$

In the same way as before, we can show that:

$$\|f(v_h) - f(v)\| \leq C\|v_h - v\| \leq C\|\theta + \rho\| \leq C(\|\theta\| + \|\rho\|). \tag{39}$$

Now, substitute (39) in (38), and using Young's inequality, we have

$$\frac{d}{dt}\|\theta\|^2 \leq C(\|\theta\|^2 + \|\rho\|^2 + \|\frac{\partial \rho}{\partial t}\|^2). \tag{40}$$

Integrating the last equation from 0 to t, gives

$$\|\theta(t)\|^2 \leq \|\theta(0)\|^2 + C\int_0^t (\|\theta(s)\|^2 + \|\rho(s)\|^2 + \|\frac{\partial \rho(s)}{\partial t}\|^2)ds. \tag{41}$$

Set $\theta(0) = 0$, and using Theorem 2.2.2, then we have

$$\|\theta(t)\|^2 \leq Ch^{2r}\int_0^t \|v(s)\|^2 ds + C\int_0^t \|\theta(s)\|^2 ds. \tag{42}$$

Using Grownwall's Theorem, we have the following

$$\|\theta(t)\|^2 \leq Ch^{2r}e^{Ct} \leq Ce^{CT}h^{2r}. \tag{43}$$

Hence,

$$\|\theta(t)\| \leq Ch^r. \tag{44}$$

So, from Equation (45) and by using Theorem 2.2.2, we have

$$\|v - v_h\| = \|\theta + \rho\| \leq \|\theta\| + \|\rho\| \leq Ch^r + Ch^{r+1}\|v\|_{r+1} \leq Ch^r(1 + \|v\|_{r+1}) \leq C(v)h^r. \tag{45}$$

2.3. Finite Element Formulation

In this section, we derive the finite element formulation corresponding to the given problem. To initiate the process, we begin by discretizing the spatial domain $[0, 1]$ into N uniform finite elements. Let

$\{x_m\}_{m=0}^{N}$ be a partition of the interval $[0,1]$ with $h=\frac{1}{N}$ and $x_m = mh$. The Lagrange function $\varphi_m(x)$ centeblack at node x_m is defined as:

$$\varphi_m(x) = \begin{cases} \frac{x-x_{m-1}}{h} & \text{for } x_{m-1} \le x \le x_m, \\ \frac{x_{m+1}-x}{h} & \text{for } x_m \le x \le x_{m+1}, \\ 0 & \text{otherwise.} \end{cases} \tag{46}$$

The derivative of $\varphi_m(x)$ is:

$$\varphi_m'(x) = \begin{cases} \frac{1}{h} & \text{for } x_{m-1} \le x \le x_m, \\ -\frac{1}{h} & \text{for } x_m \le x \le x_{m+1}, \\ 0 & \text{otherwise.} \end{cases} \tag{47}$$

Using piecewise linear basis functions $\varphi_m(x)$, we approximate $v_n(x,t)$ as:

$$v(x,t) = \sum_{j=0}^{N} \alpha_j(t)\varphi_j(x). \tag{48}$$

here $\alpha_j(t)$'s is a time dependent parameters which is going to be determined. If we use local coordinate transformation $\xi = x - x_m$, $0 \le \xi \le h$, then we obtain the Lagrange basis functions as follows:

$$\begin{matrix} \varphi_{m-1} \\ \varphi_m \end{matrix} = \begin{cases} \frac{\xi}{h}, \\ \frac{h-\xi}{h}, \end{cases} \qquad 0 \le \xi \le h. \tag{49}$$

By expressing the approximate solution (48) in terms of the local coordinate system, we obtain the following representation:

$$v_n = \sum_{j=m-1}^{m} \alpha_j^e(t)\varphi_j^e(x). \tag{50}$$

Following straightforward manipulations, the weak formulation corresponding to Equation (1) is obtained as:

$$\int_{x_m}^{x_{m+1}} \left(\frac{\partial v}{\partial t} w + \varepsilon \frac{\partial v}{\partial x}\frac{\partial w}{\partial x} + \beta v^2 w\right) dx = 0. \tag{51}$$

Since the Galerkin finite element method is employed in this study, the weight functions are selected to be the same as the basis functions, namely the Lagrange function. Substituting Equation (50) into Equation (51), we obtain the following

$$\sum_{j=m-1}^{m} \left\{ \left(\int_0^h \varphi_i \varphi_j \, d\xi\right)\dot{\alpha}_j^e + \varepsilon\left(\int_0^h \varphi_i' \varphi_j' \, d\xi\right)\alpha_j^e + \beta \sum_{k=m-1}^{m} \left(\int_0^h \varphi_i \varphi_j \varphi_k \, d\xi\right)\alpha_k^e \alpha_j^e \right\} = 0 \tag{52}$$

Upon rearranging this system into its matrix form, we arrive at the following representation:

$$M^e \dot{\alpha}^e + \varepsilon A^e \alpha^{\mathbf{e}} + \beta F^e(\alpha^{\mathbf{e}})\alpha^e = 0, \tag{53}$$

here the dot symbol denotes differentiation with respect to t, and the vectors $\alpha^e = \left(\alpha_{m-1}^e, \alpha_m^e\right)$, is treated as the local (element-wise) nodal parameter vector. The element matrices $M^e, A^e, F^e(\alpha)$ are

defined through the following integrals:

$$
\begin{aligned}
M_{ij}^{e} &= \int_0^h \varphi_i \varphi_j \, d\xi, \\
A_{ij}^{e} &= \int_0^h \varphi_i^{'} \varphi_j^{'} \, d\xi, \\
F_{ijk}^{e} &= \int_0^h \varphi_i \varphi_j \varphi_k \, d\xi.
\end{aligned} \tag{54}
$$

where $i, j, k = m-1, m$. The element matrices introduced in Equation (54) can be explicitly computed using the following expressions:

$$
M_{ij}^{e} = \frac{h}{6} \begin{bmatrix} 2 & 1 \\ 1 & 2 \end{bmatrix} \tag{55}
$$

$$
A_{ij}^{e} = \frac{1}{h} \begin{bmatrix} 1 & -1 \\ -1 & 1 \end{bmatrix} \tag{56}
$$

$$
F_{ijk}^{e} = \frac{h}{12} \begin{bmatrix} (3,1)\alpha^{e} & (1,1)\alpha^{e} \\ (1,1)\alpha^{e} & (1,3)\alpha^{e} \end{bmatrix} \tag{57}
$$

By assembling the contributions of all elements over the entire solution domain, the following system of ordinary differential equations is obtained:

$$
M\dot{\alpha} + \varepsilon A\alpha + \beta F(\alpha)\alpha = 0, \tag{58}
$$

where the global element parameter vectors are defined as $\alpha = (\alpha_0, \alpha_1, \ldots, \alpha_N)^{\intercal}$ where M, A, and $F(\alpha)$ represent the global element matrices. The generalized m^{th} row of these global matrices can be expressed as follows:

$$
M : \frac{h}{6}(1,4,1), \tag{59}
$$

$$
A : \frac{1}{h}(-1,2,-1), \tag{60}
$$

$$
F(\alpha) : \frac{h}{12}((1,1,0)\alpha, (1,6,1)\alpha, (0,1,1)\alpha). \tag{61}
$$

By using the forward finite difference approximations for $\dot{\alpha} = \dfrac{\alpha^{n+1} - \alpha^{n}}{\tau}$ and Crank–Nicolson method $\alpha = \dfrac{\alpha^{n+1} + \alpha^{n}}{2}$, equation (58) will become:

$$
M\left(\frac{\alpha^{n+1} - \alpha^{n}}{\tau}\right) + \varepsilon A\left(\frac{\alpha^{n+1} + \alpha^{n}}{2}\right) + \beta F(\alpha^{n})\left(\frac{\alpha^{n+1} + \alpha^{n}}{2}\right) = 0, \tag{62}
$$

where τ is the step size of time discretization. After simplification equation (62) blackuces to:

$$
(2M + \tau\varepsilon A + \tau\beta F(\alpha^{n}))\alpha^{n+1} = (2M - \tau\varepsilon A - \tau\beta F(\alpha^{n}))\alpha^{n}, \tag{63}
$$

In order to start the solution procedure described in Equation (63), the initial vector α^{0} must first be determined from the initial condition. Once the parameter α^{n+1} has been computed iteratively in terms of the parameter α^{n} at time t, the solution at each nodal point can then be evaluated using the expression $v(x_i, t) = \alpha_i$.

2.4. Stability Analysis of the Linearized scheme

In this section, we will study the stability analysis for the linearized scheme (63) by von Neumann method. A typical Fourier mode is described by:

$$v_j^n = \lambda^n e^{qjh\varphi}, q = \sqrt{-1}, \tag{64}$$

where j indexes the grid points, $h = \Delta x$ is the grid spacing, and the wavenumber φ represents the spatial frequency of oscillations in a wave. It determines how quickly the wave oscillates as it moves through space. The wavenumber φ is inversely related to the wavelength λ^*, with $\varphi = \frac{2\pi}{\lambda^*}$. In stability analysis, φ is crucial as it helps assess the stability of numerical schemes across different frequencies; the scheme must be stable for all possible values of φ. For the stability, the condition $|\lambda| \leq 1$ must be satisfied, for more details see the reference [1, p. 287].
To linearize our model, we assume that the quantity v in nonlinear terms v^2 is local constants, namely $\hat{v}$.
Therefore, equation (58) will be transformed into:

$$M\dot{v} + (\varepsilon A + \beta \hat{v} M)\mathbf{v} = 0, \tag{65}$$

Using the forward difference for $\dot{v}$ and Crank–Nicolson method for v, then equation (65) will become:

$$M(\frac{v^{n+1} - v^n}{\tau}) + (\varepsilon A + \beta d M)\frac{v^{n+1} + v^n}{2} = 0, \tag{66}$$

where τ is the step size of time discretization, simplify equation (66), yields:

$$(2M + \tau(\varepsilon A + \beta d M))v^{n+1} = (2M - \tau(\varepsilon A + \beta d M))v^n \tag{67}$$

The general row of M and A are $\frac{h}{6}[1\ 4\ 1]$ and $\frac{1}{h}[-1\ 2\ -1]$, respectively. So, equation (67) becomes:

$$\alpha_1 v_{j-1}^{n+1} + \alpha_2 v_j^{n+1} + \alpha_1 v_{j+1}^{n+1} = \alpha_3 v_{j-1}^n + \alpha_4 v_j^n + \alpha_3 v_{j+1}^n, \tag{68}$$

where $\alpha_1 = a_1 - a_2 + a_3$, $\alpha_2 = 4a_1 + 2a_2 + 4a_3$, $\alpha_3 = a_1 + a_2 - a_3$, $\alpha_4 = 4a_1 - 2a_2 + 4a_3$, $a_1 = \dfrac{h}{3}$, $a_2 = \dfrac{\tau\varepsilon}{h}$ and $a_3 = \dfrac{\tau d\beta h}{6}$.
Now, put equation (64) in equation (68). After simplification, we will get:

$$\lambda(\alpha_1 e^{-i\varphi h} + \alpha_2 + \alpha_1 e^{i\varphi h}) = \alpha_3 e^{-i\varphi h} + \alpha_4 + \alpha_3 e^{i\varphi h} \tag{69}$$

We will use the Euler's formula $e^{q\theta} = \cos(\theta) + q\sin(\theta)$, then equation (69) blackuces to:

$$\lambda = \frac{\alpha_4 + 2\alpha_3\cos(\varphi h)}{\alpha_2 + 2\alpha_1\cos(\varphi h)} \tag{70}$$

Because $|\lambda| \leq 1$ is the stability condition. One way to rewrite this condition is as follows:

$$\lambda^2 \leq 1 \tag{71}$$

Equation (70) is used to transform the inequality equation (71) into:

$$(\alpha_4 + 2\alpha_3\cos(\varphi h))^2 \leq (\alpha_2 + 2\alpha_1\cos(\varphi h))^2 \tag{72}$$

Thus, we have:

$$\left(\frac{4h}{3}+\cos(h\varphi)\left(\frac{2h}{3}+\frac{2\varepsilon\tau}{h}-\frac{dh\beta\tau}{3}\right)-\frac{2\varepsilon\tau}{h}+\frac{dh\beta\tau}{3}\right)^2$$
$$\leq\left(\frac{4h}{3}+\cos(h\varphi)\left(\frac{2h}{3}-\frac{2\varepsilon\tau}{h}+\frac{dh\beta\tau}{3}\right)+\frac{2\varepsilon\tau}{h}+\frac{dh\beta\tau}{3}\right)^2$$

After simplification we will get:

$$\left(4h^2+\cos(h\varphi)\left(2h^2+6\varepsilon\tau-dh^2\beta\tau\right)-6\varepsilon\tau+dh^2\beta\tau\right)^2$$
$$\leq\left(4h^2+\cos(h\varphi)\left(2h^2-6\varepsilon\tau+dh^2\beta\tau\right)+6\varepsilon\tau+dh^2\beta\tau\right)^2$$

If we take h sufficiently small s.t. $h\to 0$, then the inequality holds and the stability condition (71) holds for equation (67).

3. Numerical Results

This section presents the numerical findings derived from the finite element method (FEM) that applied to the nonlinear reaction-diffusion problem (1) that investigated in this study, to conduct a convergence study numerically with respect to temporal discretization, with parameters $\varepsilon=0.01$ and $\beta=2$. The spatial domain $x\in[0,1]$, while the temporal domain $t\in[0,1]$ was investigated with five progressively refined time steps: $\Delta t_1=0.02$, $\Delta t_2=0.01$, $\Delta t_3=0.005$, $\Delta t_4=0.002$, and $\Delta t_5=0.001$. The convergence numerically was assessed by computing pairwise absolute differences between solutions obtained with consecutive time steps:

$$E_1=|v_{\Delta t_1}-v_{\Delta t_2}| \quad (\Delta t=0.02 \text{ vs } 0.01)$$
$$E_2=|v_{\Delta t_2}-v_{\Delta t_3}| \quad (\Delta t=0.01 \text{ vs } 0.005)$$
$$E_3=|v_{\Delta t_3}-v_{\Delta t_4}| \quad (\Delta t=0.005 \text{ vs } 0.002)$$
$$E_4=|v_{\Delta t_4}-v_{\Delta t_5}| \quad (\Delta t=0.002 \text{ vs } 0.001)$$

Table 1: Absolute differences between FEM solutions at $t=0.1$ for all time step comparisons.

x	$E_1\times10^{-5}$	$E_2\times10^{-5}$	$E_3\times10^{-5}$	$E_4\times10^{-5}$
0	0	0	0	0
0.1	542.55020787	246.78916531	142.81253641	46.77695829
0.2	15.84767036	6.17538077	2.95569569	0.85327364
0.3	3.60509260	1.79549811	1.07550583	0.35818950
0.4	0.51342363	0.25936528	0.15647039	0.05229857
0.5	0.08598083	0.04280338	0.02561221	0.00852495
0.6	0.09349461	0.04739481	0.02863975	0.00958003
0.7	0.03688084	0.01898877	0.01156649	0.00388423
0.8	0.00156337	0.00263629	0.00222374	0.00085053
0.9	0.01522218	0.00391795	0.00091677	0.00007093
1	0	0	0	0

Table 1 shows spatial errors, peaking in the left interior before decaying rightward. Finer resolutions yield systematically smaller differences, while zero boundary errors confirm correct implementation. The results validate the numerical method.

Figure 1 presents both the solution profiles at $t = 0.1$ (Top panel) and these difference measures (Bottom panel). The solution curves demonstrate clear convergence as the time step decreases, while the difference plots show the expected blackuction in discrepancy with temporal refinement.

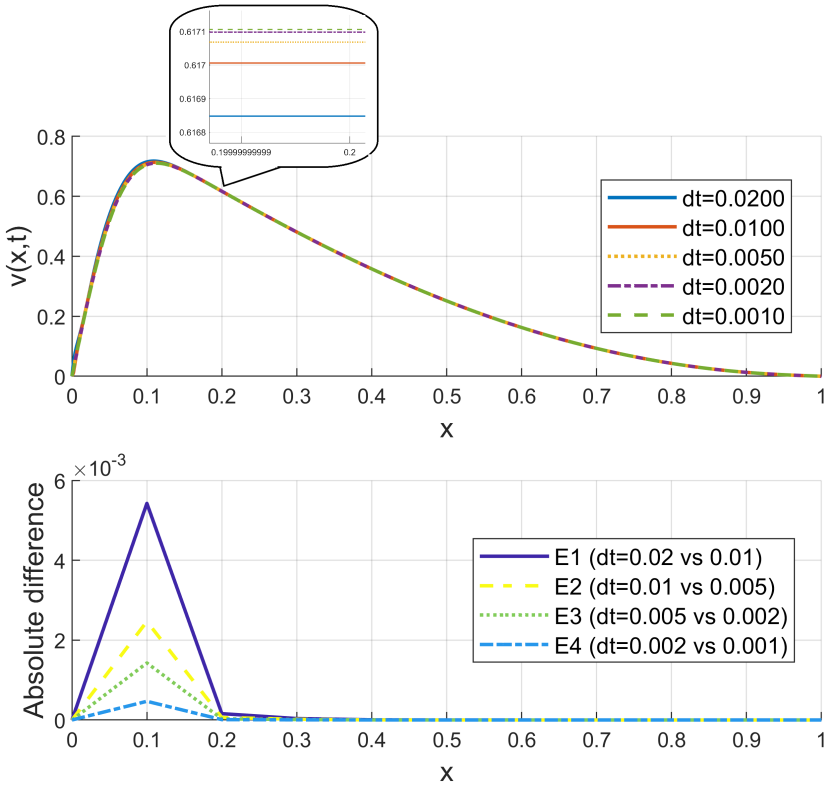

Figure 1: (Top) FEM solutions at $t = 0.1$ for all five time steps. (Bottom) Absolute differences between consecutive time step solutions (E_1 through E_4).

Table 2: Finite element method solution of the equation (1) with different values of the parameters ε and β.

	$\varepsilon = 0.01$ and $\beta = 0.1$		$\varepsilon = 0.1$ and $\beta = 10$		$\varepsilon = 0.01$ and $\beta = 20$	
x	$t = 0.5$	$t = 1$	$t = 0.5$	$t = 1$	$t = 0.5$	$t = 1$
0	0	0	0	0	0	0
0.1	0.17494067	0.10780233	0.03287039	0.01377354	0.05129201	0.02566614
0.2	0.32545770	0.20578839	0.06064626	0.02615666	0.09343665	0.04825182
0.3	0.44525090	0.29326289	0.08295811	0.03699278	0.12686608	0.06861673
0.4	0.52349402	0.36320325	0.09970559	0.04590461	0.14919166	0.08491019
0.5	0.56118196	0.41228803	0.11160333	0.05283001	0.16187046	0.09659098
0.6	0.56840255	0.44360293	0.12076256	0.05843430	0.16859654	0.10525958
0.7	0.55272394	0.45708032	0.12755630	0.06278338	0.17075438	0.11080968
0.8	0.52379297	0.45554417	0.13223484	0.06596487	0.17006534	0.11376768
0.9	0.48686101	0.44251121	0.13578983	0.06847901	0.16744304	0.11498649
1	0.44684093	0.42087769	0.13801614	0.07028339	0.16347607	0.11469972

Based on the Finite Element Method solutions presented in the Table 2 for the nonlinear reaction-diffusion equation, the results demonstrate a clear dependence of the reactant concentration profile on the parameters ε (diffusion rate) and β (reaction rate). For the case with low diffusion and a very

low reaction rate ($\varepsilon = 0.01, \beta = 0.1$), the concentration values are the highest overall, exhibiting a distinct spatial peak and a significant decrease over time from $t = 0.5$ to $t = 1$, which is characteristic of a diffusion-influenced process. In contrast, the scenario with high diffusion and a high reaction rate ($\varepsilon = 0.1, \beta = 10$) yields the lowest concentration values, with a relatively flat profile and minimal change over time, indicating that the reactant is rapidly and almost uniformly consumed. The case with low diffusion but a very high reaction rate ($\varepsilon = 0.01, \beta = 20$) shows an intermediate concentration level, where the intense reaction is somewhat constrained by limited diffusion, leading to a more pronounced spatial variation than the high-diffusion case but faster consumption than the low-reaction case. These results effectively capture the interplay between diffusion and reaction in shaping the concentration dynamics within the catalytic pellet.

A comparison study is performed between our result and the FDM of the reference [22] to confirm the results. Table 3 presents numerical values of $v(x,t)$ at various time instances ($t = 0.1$, $t = 0.5$, and $t = 1$), showing the agreement between the two techniques. Figure 2 illustrates a visual comparison of the solutions obtained from our results of FEM and the approximate solution by FDM in [22], while Figure 3 presents the variation of $v(x,t)$ across the spatial domain at various time occurrences. The findings validate the accuracy and stability of the FEM, further corroborating its theoretical robustness through close agreement with the FDM results.

Table 3: Comparison of FEM and FDM of the equation (1) with $\varepsilon = 0.01$ and $\beta = 0.5$.

	$t = 0.1$		$t = 0.5$		$t = 1$	
x	FEM	FDM	FEM	FDM	FEM	FDM
0	0	0	0	0	0	0
0.1	0.40576546	0.42782018	0.13067720	0.12385283	0.07104334	0.06199795
0.2	0.63291799	0.65072408	0.24055922	0.22764969	0.13442787	0.11784450
0.3	0.70105577	0.69660344	0.32710304	0.30215063	0.19069795	0.16382127
0.4	0.67695008	0.65312090	0.38396477	0.34724458	0.23540191	0.19853511
0.5	0.63718653	0.61033239	0.41335538	0.36799991	0.26697929	0.22230741
0.6	0.59271267	0.56832782	0.42317165	0.37116179	0.28853312	0.23646407
0.7	0.54843896	0.52719697	0.41788952	0.36296698	0.29997947	0.24275003
0.8	0.50653618	0.48702922	0.40335779	0.34816853	0.30294734	0.24293505
0.9	0.46447422	0.44791320	0.38252614	0.32988939	0.29945458	0.23859232
1	0.42375550	0.40993650	0.35835597	0.30992510	0.29073950	0.23100409

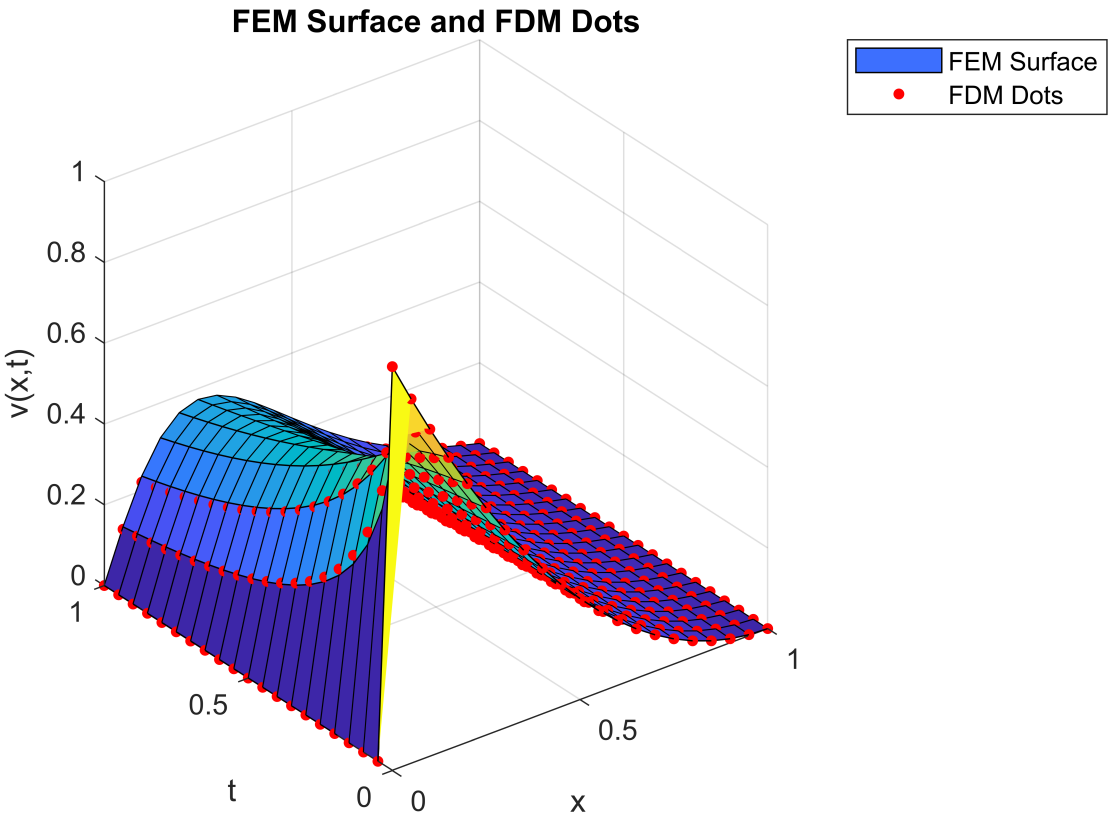

Figure 2: FEM and FDM solutions $v(x,t)$ for the catalytic pellet model with $\varepsilon = 0.01$ and $\beta = 0.5$.

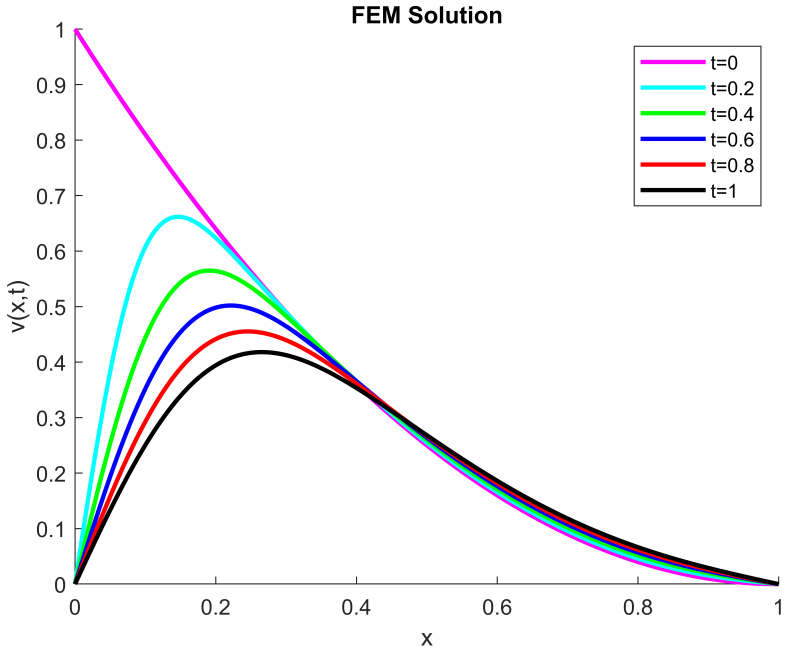

Figure 3: The Variation in $v(x,t)$ at different time instances for the catalytic pellet model with $\varepsilon = 0.01$ and $\beta = 0.5$.

4. Conclusion

This study underscores the theoretical rigor and computational efficacy of the FEM in solving nonlinear reaction-diffusion equations, particularly as applied to catalytic pellet models. The weak formulation of the given partial differential equation provided a mathematically robust framework, over Sobolev spaces to establish the existence and uniqueness of solutions. The Galerkin approximation, central to the FEM implementation, was instrumental in developing semi-discretized and fully discretized formulations, accompanied by a priori error estimates and convergence analyses. These results confirm the theoretical robustness of FEM and its capability to provide reliable approximations for complex systems.

The stability of the FEM implementation, analyzed within the Crank–Nicolson framework, further demonstrated the method's robustness, ensuring that the discretized solutions remain consistent and stable under temporal and spatial variations. The use of piecewise linear basis functions for spatial discretization allowed for precise representation of the system's dynamics, highlighting the versatility of FEM in handling boundary conditions and irregular geometries.

The comparative analysis with the FDM validated the numerical results and emphasized FEM's theoretical advantages, such as its ability to handle weak solutions and accommodate nonlinearity effectively. The close agreement between FEM and FDM results reinforced the accuracy of the numerical solutions while demonstrating FEM's superior adaptability and theoretical robustness for solving reaction-diffusion equations. Therefore, the FEM proves to be a theoretically grounded and computationally efficient approach for the approximate solution of nonlinear partial differential equations. Its rigorous mathematical formulation, coupled with demonstrated stability and convergence properties, makes FEM a cornerstone technique in numerical analysis, particularly for systems governed by reaction-diffusion dynamics in engineering and applied sciences. In the future, we intend to broaden the application of the Haar wavelet collocation method to various challenging real-world problems, for more details see [25, 24].

Author's Contribution

The authors contributed equally to this work; form the implementation and design of the research, to the analysis of the results, and to the writing of the manuscript.

Conflict of Interest

There is no conflict of interest for this paper.

Acknowledgment

The authors thank Koya University for their financial assistance.

References

[1] El Danaf, T. S. Efficient and accurate numerical treatment of Huxley equation. *International Journal of Numerical Methods for Heat & Fluid Flow*. 2011, 21(3), 282–292. https://doi.org/10.1108/09615531111108468.

[2] Sadeeq, M. I. & Sabawi, Y. A. Cubic B-spline finite element method for solving Whitham-Broer-Kaup shallow water model. *International Journal of Computational Methods*. 2025. https://doi.org/10.1142/S021987622550032X.

[3] Thomée, V. *Galerkin Finite Element Methods for Parabolic Problems*. 2nd ed. Berlin: Springer-Verlag, 2006. https://link.springer.com/book/10.1007/3-540-33122-0.

[4] Atouani, N. & Omrani, K. Galerkin finite element method for the Rosenau-RLW equation. *Computers & Mathematics with Applications*. 2013, 66(3), 289–303. https://doi.org/10.1016/j.camwa.2013.04.029.

[5] Ciarlet, P. G. *The Finite Element Method for Elliptic Problems*. Philadelphia, PA: Society for Industrial and Applied Mathematics, 2002.

[6] Chung, S. K. & Ha, S. N. Finite element Galerkin solutions for the Rosenau equation. *Applicable Analysis*. 1994, 54(1-2), 39–56. https://doi.org/10.1080/00036819408840267.

[7] Hartman, P. *Ordinary Differential Equations*. SIAM, 2002.

[8] Sabawi, Y. A. A posteriori error analysis in finite element approximation for fully discrete semilinear parabolic problems. In *Finite Element Methods and Their Applications*. IntechOpen, 2020. https://doi.org/10.5772/intechopen.94369.

[9] Sabawi, Y. A. A Posteriori $L_\infty(L_2)$ + $L_2(H^1)$–Error bounds in discontinuous galerkin methods for semidiscrete semilinear parabolic interface problems. *Baghdad Science Journal*. 2021, 18(3), 0522. https://doi.org/10.21123/bsj.2021.18.3.0522.

[10] Pirdawood, M. A. & Sabawi, Y. A. High-order solution of Generalized Burgers–Fisher Equation using compact finite difference and DIRK methods. *Journal of Physics: Conference Series*. 2021, 1999, 012088. https://doi.org/10.1088/1742-6596/1999/1/012088.

[11] Sabawi, Y. A., Pirdawood, M. A. & Sadeeq, M. I. A compact fourth-order implicit-explicit Runge-Kutta type method for solving diffusive Lotka–Volterra system. *Journal of Physics: Conference Series*. 2021, 1999, 012103. https://doi.org/10.1088/1742-6596/1999/1/012103.

[12] Cangiani, A., Georgoulis, E. H. & Sabawi, Y. A. Convergence of an adaptive discontinuous Galerkin method for elliptic interface problems. *Journal of Computational and Applied Mathematics*. 2020, 367, 112397.

[13] Cangiani, A., Georgoulis, E. & Sabawi, Y. Adaptive discontinuous Galerkin methods for elliptic interface problems. *Mathematics of Computation*. 2018, 87(314), 2675–2707.

[14] Evans, L. C. *Partial Differential Equations*. 2nd ed. American Mathematical Society, 2022.

[15] Brezis, H. *Functional Analysis, Sobolev Spaces and Partial Differential Equations*. Springer Science & Business Media, 2011.

[16] Al-Bairaqdar, O.T., Sabawi, Y.A. and Hasso, M.S., 2025. Efficient numerical solution of the Allen–Cahn equation via a non-lumping Galerkin finite element method. AIP Advances, 15(7). https://doi.org/10.1063/5.0262503.

[17] Quarteroni, A. *Numerical Models for Differential Problems*. Vol. 2. Springer, 2009.

[18] Kesavan, S. *Topics in Functional Analysis and Applications*. 1989.

[19] Cho, Y. Modeling of Cone-Shaped Pellets for Catalytic Reactors. *Journal of Chemical Engineering of Japan*. 2024, 57(1), 2317457. https://doi.org/10.1080/00219592.2024.2317457.

[20] Cho, Y. Modeling of porous catalytic pellets with various morphologies suspended in batch reactor and CSTR from analytical solutions of reaction-diffusion equations. *Journal of Chemical Engineering of Japan*. 2023, 56(1), 2247783. https://doi.org/10.1080/00219592.2023.2247783.

[21] Kreyszig, E. *Introductory Functional Analysis with Applications*. John Wiley & Sons, 1991.

[22] Rufai, M. A., Carpentieri, B. & Ramos, H. A New Hybrid Block Method for Solving First-Order Differential System Models in Applied Sciences and Engineering. *Fractal and Fractional*. 2023, 7(10), 703. https://doi.org/10.3390/fractalfract7100703.

[23] Tannhäuser, K., Serrao, P. H. & Kozinov, S. A three-dimensional collocation finite element method for higher-order electromechanical coupling. *Computers & Structures*. 2024, 291, 107219. https://doi.org/10.1016/j.compstruc.2023.107219.

[24] Mohammad, N. A., Sabawi, Y. A. & Hasso, M. S. Numerical solution based on the Haar wavelet collocation method for partial integro-differential equations of Volterra type. *Arab Journal of Basic and Applied Sciences*. 2024, 31(1), 614–628. https://doi.org/10.1080/25765299.2024.2419145.

[25] Mohammad, N. A., Sabawi, Y. A. & Hasso, M. S. A compact finite-difference and Haar wavelets collocation technique for parabolic volterra integro-differential equations. *Physica Scripta*. 2024, 99(12), 125251. https://doi.org/10.1088/1402-4896/ad8d3d.

[26] Hellman, F., Målqvist, A. & Mosquera, M. Well-posedness and finite element approximation of mixed dimensional partial differential equations. *BIT Numerical Mathematics*. 2024, 64(1), 2. https://doi.org/10.1007/s10543-023-01001.